Revisiting hollandites: channels filling by main-group elements together with transition metals in Bi2-yVyV8O16

Lebedev, O. I.; Hébert, S.; Roddatis, V.; Martin, C.; Turner, S.; Krasheninnikov, A. V.; Grin, Y.; Maignan, A.;

Perma-Link to Publication Repository of HZDR:

https://www.hzdr.de/publications/Publ-25690

Revisiting hollandites:

channels filling by main-group elements together with transition metals

in $Bi_{2-y}V_yV_8O_{16}$

O. I. Lebedev[1], S. Hébert[1], V. Roddatis[2], C. Martin[1], S. Turner[3],

A.V. Krasheninnikov[4,5,6], Y. Grin[7], and A. Maignan[1*]

[1]Laboratoire CRISMAT, UMR 6508 CNRS/ENSICAEN/UCBN, 6 bd du Maréchal Juin, F-14050 CAEN Cedex 4 – France

[2] Institut für Materialphysik Universität Göttingen, Friedrich-Hund-Platz 1, 37077 Göttingen

[3] EMAT, Department of Physics, University of Antwerp, B-2020, Antwerp, Belgium

[4] Helmholtz-Zentrum Dresden-Rossendorf, Institute of Ion Beam Physics and Materials Research, 01328 Dresden, Germany

[5] Department of Applied Physics, Aalto University, P.O. Box 1100, 00076 Aalto, Finland

[6] National University of Science and Technology MISiS, 4 Leninskiy prospekt, Moscow, 119049, Russian Federation

[7] Max-Planck-Institut für Chemische Physik fester Stoffe, Nöthnitzer Straße 40, 01187 Dresden, Germany

Abstract

Starting from the nominal $Bi_xV_8O_{16}$ formula, state-of-the-art transmission electron microscopy investigation has been made to propose the new chemical formula $Bi_{2-y}V_yV_8O_{16}$ for this hollandite structure. This results from the filling of the channels by main-group elements together with vanadium (V^{5+}) species, with variable content of Bi and V inside the channels. The influence of the Bi content and of this local disorder on the magnetic and transport properties has been investigated in polycrystalline samples of $Bi_xV_8O_{16}$ with nominal composition x = 1.6 and x = 1.8. The rather x-independent electrical resistivity (≈ 5 mΩ·cm) and Seebeck coefficient at high T (-35 µV·K^{-1} at 900 K) is discussed in terms of an unchanged V oxidation state resulting from the filling-up of the wide channels with Bi and V. It is proposed that this local disorder hinders the charge/orbital setting below 60 K on the V ions of the V_8O_{16} framework. Hollandites exhibit complex electronic and magnetic properties with potential applications in the field of batteries, photocatalysis or nuclear waste storage, and these results show that a careful and detailed investigation of the nature and content of the cations inside the channels is crucial to better understand the doping and disorder impact on their properties.
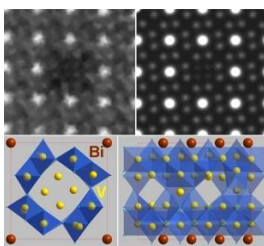
*Corresponding Author
Sylvie HEBERT
Laboratoire CRISMAT, ENSICAEN/CNRS, 6 boulevard du Maréchal Juin, 14050 Caen cedex 4 - France
sylvie.hebert@ensicaen.fr
Tel: 33.(0)2.31.45.29.10

Introduction

The hollandite family with the chemical composition $A_xM_8O_{16}$ (A = K, Pb, Ba, Bi, Ag, …) containing magnetic transition metals (M) with mixed valence exhibit a wide range of interesting physical properties related to electronic correlations, magnetic frustration and orbital ordering [1-14]. The M_8O_{16} framework with different kinds of 1D channels allows insertion and release of cations or small molecules in the wider tunnels making hollandites interesting candidates for several applications as electroactive cathode [15], photocatalysis[16-17], or as host material for bearing radioactive ions[18-19].

The building unit of this crystal structure consists of stripes made up of infinitely stacked edge-sharing MO_6 octahedra, which share corners to form a M_8O_{16} framework with wide and narrow tunnels. The average formal oxidation state of M is tetravalent. The wide tunnels are occupied in commensurate or incommensurate manner by A^{n+} cations up to a maximum of $x = 2$ (figure 1b). The charge transfer from the A^{n+} cations to the M_8O_{16} hollandite network generates a M^{3+}/M^{4+} mixed valence for the M species. In the M_8O_{16} network, these extra electrons order in a 1D pattern leading to complex M-M magnetic exchange pathways, with frustration in the M_3 triangles (see Fig. 1c, with $Bi_xV_8O_{16}$ for x =1.625). Through corner sharing oxygen atoms bridging the stripes, there exists an additional magnetic exchange between the zigzag chains along the stripes [12]. Moreover, the tetragonal crystal structure is likely to exhibit distortions, and can become monoclinic, with the large tunnels that do not longer have the square shape, or with the Mo_4 "clusters" in $(MoO_6)_2$ stripes [5]. The tetragonal-to-monoclinic transition combined with charge/orbital ordering is responsible for the metal-to-insulator transition (MIT) in $K_2V_8O_{16}$ and $K_2Cr_8O_{16}$ [2-3, 14]. The complex properties of these hollandites has stimulated experimental and theoretical investigations to better understand the strong coupling between the lattice, spins and charges[1-14], and the role of the frustration inside the ribbons on magnetism[12-13]. The defects chemistry inside the channels has also been found to play a major role on the properties such as ionic conductivity[20], or on the resistivity of Ru hollandites[21]. The filling mechanism inside the channels of these hollandites needs to be well understood to better analyze the doping effect and possible disorder impact.

Despite all these features, only a moderate activity has been focused on local atomic arrangements in hollandites and their correlation with the properties, applying in particular the state-of-the- art transmission electron microscopy. To the best of our knowledge, only few

reports have been published [20, 22-24] in the last twenty years. M.L.Carter et al. presented extensive studies on barium titanate $Ba_xM_yTi_{8-y}O_{16}$ by electron diffraction and appearance of modulated structures.[22-23] L.Nistor et al reported high resolution transmission electron microscopy and electron diffraction studies of defects in the natural hollandite $Ba_xMn_8O_{16}$ and found as a main structural feature shear plane defects.[24] The different arrangements of these defects were attributed to commensurate and incommensurate modulations in ED patterns. We did not find in the literature results of detailed studies of the reasons for these structural features with atomic resolution.

For vanadium-based hollandites only, a MIT for all of them has been evidenced with a coupled magnetic transition at 180 K for $K_2V_8O_{16}$ [2], 140 K for $Pb_{1.6}V_8O_{16}$ [10] and near 60 K for $Bi_{1.8}V_8O_{16}$ [7]. Considering the filling level of the wider tunnel, the formal oxidation state of vanadium is larger than 3.5 for the two first ($v_V = 3.75$ and 3.60 for $K_2V_8O_{16}$ and $Pb_{1.6}V_8O_{16}$, respectively), but smaller for $Bi_{1.8}V_8O_{16}$ with $v_V = 3.325$. This correlates with the lower T_{MIT} for the bismuth hollandite. Additionally, the coexistence of a rather constant resistivity at high T (from 300 to 1000 K) together with a continuous increase of $|S|$ up to 1000 K in $Pb_{1.6}V_8O_{16}$ motivates a more detailed investigation of physical properties of synthetic hollandites as a function of x. The $Bi_xV_8O_{16}$ bismuth vanadate ($1.6 \leq x \leq 1.8$) [7, 8, 25-26] is well worth studying for its structural features and their impact on magnetic and transport properties.

In the following, we report the evidence of a simultaneous filling of channels by main-group elements and transition metals in $Bi_{2-y}V_yV_8O_{16}$ and its possible linking with the physical properties. The crystal structure has been characterized by atomic-resolution transmission electron microscopy. The wider tunnels of the hollandite structure are not only partially occupied by Bi^{3+} but also contain tetrahedrally coordinated vanadium cations, a result which is supported by electronic structure calculations. The vanadium oxidation state determined by EELS and its relation with the Seebeck coefficient is also discussed.

Experimental section

Polycrystalline samples of $Bi_xV_8O_{16}$ with x values in the range of $1.6 \leq x \leq 1.8$ have been synthesized by solid state reaction. According to the nominal composition $Bi_xV_8O_{16}$, stoichiometric amounts of Bi_2O_3, V_2O_3 and V_2O_5 were mixed in a glove box and pressed in bar-shaped specimen ($2 \times 2 \times 10$ mm). An alumina crucible containing the bars was sealed in a silica tube under primary vacuum. The ampoule was heated at 1000 °C for 12 hours and

subsequently cooled down to room temperature in 6 hrs. The obtained black product was characterized by room temperature (RT) X-ray powder diffraction (XRD, CuK$_\alpha$ radiation) and transmission electron microscopy.

Specimens for electron microscopy studies were ground in methanol and drop cast onto a holey carbon film fixed on a 3 mm copper grid. Transmission electron microscopy (TEM) and electron diffraction (ED) studies were performed using FEI Tecnai G2 30 UT microscope operated at 300 kV, with a point resolution of 0.17 nm. High resolution high-angle annular dark-field STEM (HAADF-STEM) experiments were carried out by using an aberration double-corrected JEM ARM200F microscope operated at 200 kV equipped with a CENTURIO EDX detector and GIF Quantum spectrometer. Electron energy-loss spectroscopy experiments (EELS) were performed on Titan "cubed" microscope, equipped with an electron monochromator and a GIF Quantum spectrometer, operated at 120 kV in scanning TEM mode. The monochromator provided an energy resolution of 200 meV. The convergence semi-angle α was 18 mrad, the acceptance inner semi-angle β was 130 mrad. Atomic models for simulation were built using Atoms 6.4, CrystalMaker and the Vesta [27] software packages. The high resolution HAADF-STEM simulated images were calculated using the QSTEM package [28].

Magnetic measurements were performed by SQUID magnetometer. For T < 325 K, the four-probe technique and steady-state method were used for electrical resistivity (ρ) and Seebeck (S) coefficient measurements, respectively. Above that temperature, a ULVAC ZEM3 system was used to perform simultaneous measurements of ρ and S in an inert gas atmosphere.

The first-principles calculations were carried out using the Vienna *Ab-initio* Simulation Package (VASP) [29-30] software on CRAY XC40 supercomputer. We used the generalized gradient approximation with the Perdew-Burke-Ernzerhof [31] parameterization and the projected augmented wave [32] approach to describe core electrons. A rectangular 2×2×4 supercell was used. The larger supercells can hardly be studied with the same accuracy due to computational limitations even on the CRAY XC40 supercomputer.

Results and discussion

Structure characterization by XRD

X-ray powder diffraction (x = 1.6 in Fig. 1a) confirms the hollandite structure with the space group $I4/m$ reported for a $Bi_{1.625}V_8O_{16}$ single crystal [25- 26]. The unit cell parameters $a = 9.9323(2)$ Å and $c = 2.9128(1)$ Å (V = 287.35(1) Å^3) of the material with the nominal composition $Bi_{1.6}V_8O_{16}$ are close to the previously reported $a = 9.930(4)$ Å and $c = 2.914(1)$ Å (V = 287.33 Å^3) [25- 26]. Increasing the x value up to 1.8 in the starting mixture of precursors slightly increases the unit cell volume with decreasing a parameter and increasing c parameter: a = 9.9225(2) Å, c = 2.9230(1) Å and V = 287.78(1) Å^3. No significant impurities were detected in XRD patterns for all samples.

TEM studies

The hollandite-type crystal structure of $Bi_{1.625}V_8O_{16}$ comprises a network of double rutile-like ribbons of edge-sharing VO_6 octahedra sharing corners and forming the wide square channels occupied by Bi^{3+} cations (Fig. 1b).

Figure 2a-b shows the electron diffraction (ED) patterns along the most informative zone axes [001]*, [100]* and [111]* for $Bi_{1.8}V_8O_{16}$. The ED patterns were completely indexed using the space group $I4/m$ (no. 87) and the unit cell parameters determined by powder XRD. No significant differences were observed in ED pattern for different x values which is in good agreement with the conclusions from powder XRD data. The HRTEM study of $Bi_{1.8}V_8O_{16}$ (Fig. 2b) was performed along the most informative [001] zone along wide tunnels. It exhibits uniform contrast, free of any modulation and defects within the single crystallites. No superstructure features resulting from long-range ordering were observed as well. However, a careful analysis of ED patterns (Fig.2a) revealed the appearance of diffuse streak lines normal to c* axis and parallel to the $h0l$ spots rows in all [100]* and [111]* ED patterns which can be interpreted in terms of short-range ordering of Bi vacancies in the incommensurate structure. A similar behaviour was observed previously in barium titanate hollandites [23] and attributed to A cations ordering along the tunnel direction. In order to shed light on these features the state-of-the-art TEM microscopy was applied. The direct interpretation of HRTEM images of a complex compound with a large unit cell is not always straightforward. The phase-contrast image formation in HRTEM is not very sensitive to small compositional variations within a single atomic column. To overcome these drawbacks, incoherent HAADF-STEM imaging, so called 'Z-contrast' was used to clarify the crystal structure model of $Bi_xV_8O_{16}$ and determine possible structural or/and compositional variations at the atomic level. The contrast in HAADF-STEM is roughly proportional to the thickness of the specimen and square atomic

number Z^2 of the components, making it possible to detect even small changes in the composition and positions of Bi (Z = 83) or/and V (Z = 23).

High resolution HAADF-STEM images of the nominal $Bi_{1.8}V_8O_{16}$ structure along [001] and [100] zone axis are shown in Figure 3. The columns of Bi and V atoms can easily be distinguished in the [001] image (Fig. 3a): the brightest square-arranged dots correspond to the Bi atomic columns (Z = 83) whereas the eight less bright dots surrounding each Bi atomic column are *V* atomic columns (Z = 23). The same definition applies to [100] HAADF-STEM image (Fig. 3b) where brightest dots correspond to row of Bi atoms and less bright to V atoms in between the layers. Importantly, the Fourier transformation (FT) of the [100] image reproduces diffuse line normal to *c**-axis similar to that of ED pattern (Fig. 2a). A careful inspection of the images reveals the presence of numerous inhomogeneities in the local contrast along both zone axes. The contrast in the vanadium columns does not change markedly over the whole region of the HAADF-STEM image, whereas the contrast in the vicinity of the Bi columns in the wide channels varies strongly. It appears as a complete lack of contrast in [001] image (Fig. 3a) or more frequently as a significant reduction in intensity in both directions (Fig. 3a,b) in comparison with the regular contrast of neighboring Bi atomic columns as we can see from intensity plot profile in Figure 3c. The 'split' of the Bi spots in the view along [100] is caused by different orientation of the incommensurate Bi chains (starting coordinates z and –z) and shift of the Bi atoms from the tunnel axis. The careful analysis of [100] high resolution HAADF-STEM image (Fig. 3d) also reveals a lack of Bi atoms in the expected positions reflecting their partial occupancy.

In the [001] image (Fig.3a), the contrast within the wide channel (Bi columns) can be absent, as shown by the arrow. Instead, a square arrangement of lower contrast intensity appears displaying contrast similar to the other V columns and suggesting the presence of additional V atoms inside the wide channels (Fig.4b). The filling of channels by the same element as in the octahedral framework is observed for the first time in hollandite materials and may be important in the understanding of their physical properties. It should be noticed that A-cation vacancies were recently reported in nanorods of silver hollandite $Ag_xMn_8O_y$ [20], but no Mn was detected inside empty channels. In this regard, an important question arises about the real atomic arrangements in the wide channels and how they are related to the structure of the nominal $Bi_{1.8}V_8O_{16}$.

The structural model which allows the simulation of different situations within the wide channels was constructed starting with the reported crystal structure data of $Bi_{1.625}V_8O_{16}$ [25-26] as follows. The symmetry of the structure was chosen to $P4_1$ with the unit cell parameters

from the model are $a = a_{Bi1.625V8O16}$ and $c = 4c_{Bi1.625V8O16}$. At the first stage, the positions of the vanadium and oxygen atoms from the single crystal structure determination were used without changes. The bismuth atoms were located along the wide channel axis at $00z$ and $\frac{1}{2}\frac{1}{2}z$ with the primary shift by $0.1045c_{Bi1.625V8O16}$ and $0.6045c_{Bi1.625V8O16}$ taking into account the position of Bi atoms found in the X-ray diffraction experiment [25-26]. This model 1 with the ideal composition $Bi_2V_8O_{16}$ describes well the HAADF-STEM contrast in many regions of the experimental image (Fig. 4a). The case of the complete absence of bismuth atoms in one of the channel at the $\frac{1}{2}\frac{1}{2}z$ is described with model 2 (lattice parameters as in model 1). Here, the $00z$ axis is occupied by Bi atoms as in model 1 (Fig. 4b), and the additional V ions are located at the channel of Bi- missing atoms, leading to the limit hypothetical$Bi_1V_1V_8O_{16}$. The additional vanadium atoms are located around the $\frac{1}{2}\frac{1}{2}z$ axis replacing the missing Bi, close to the wall of the channel employing the available oxygen atoms to form tetrahedral environment and yielding the composition $Bi_1V_1V_8O_{16}$. In order to keep V-O distances in reasonable limits, the oxygen atoms were slightly shifted from their ideal positions in the crystal structure of $Bi_{1.7}V_8O_{16}$. A maximum intensity search was used to find the positions of atomic columns of additional vanadium and adjacent oxygens. The calculated and experimental HAADF-STEM contrasts for model 2 are shown in Figure 4b.

For modelling the mixed occupation of the $\frac{1}{2}\frac{1}{2}z$ axis (models 3 and 4), the unit cell have to be doubled in the [001] direction: $a = a_{Bi1.7V6O18}$ and $c = 8c_{Bi1.7V6O18}$ (Figure 4c). The V/Bi ratio on the $\frac{1}{2}\frac{1}{2}z$ axis is 3/1 (model 3) or 2/2 (model 4). In order to keep large enough distance of Bi to the vanadium in this channel, the bismuth atoms were shifted from the axis toward the wall. Both models 3 (composition $Bi_{1.25}V_{0.75}V_8O_{16}$) and 4 (composition $Bi_{1.5}V_{0.5}V_8O_{16}$) describe well fine details of contrast in the experimental HAADF-STEM images (Figures 4c and 4d). .

In order to confirm the stability of the proposed defect structure, we carried out first-principles calculations within the framework of the density functional theory. The defect structure was modeled as a rectangular $2\times2\times4$ supercell where a column of Bi atoms was replaced with V (Fig. 5). The supercell with such defect configuration contained 28 Bi, 256 O and 132 V atoms (in total 416 atoms). Such defect configuration was found to be stable, as also confirmed by repeating the calculations with initial random displacement of all the atoms within 0.1 Å. The zoomed panel in Figure 5 on the right-hand side shows the details of the atomic structure in the defect area. It is evident that atoms $V_1 - V_4$ are located at different 'heights', which breaks the symmetry and gives rise to the changes in the positions of neighboring Bi atoms as observed in Fig. 3d. This effect may be in part due to spurious

interaction between the images of the defects, as the supercell used was rather small. We also found a metastable configuration where atoms $V_1 - V_4$ were displaced by about 0.3 Å away from the center of the channel, but this configuration was higher in energy by 1.3 eV. The TEM images simulated using the DFT-optimized geometry for the input, proved to be in a good agreement with the experimental data.

The final composition in case of such Bi-by-V substitution is $V_2V_8O_{16}$, i.e. $V_{10}O_{16}$, this would yield the average valence of $v_V = 3.2$ and whereby the tetrahedral coordination of the additional position put into mind a possible presence of pentavalent vanadium.

Electronic state of vanadium

To probe the change of the V oxidation state with Bi content x, electron energy loss spectroscopy (EELS) was performed on three $Bi_xV_8O_{16}$ samples with nominal $x = 1.6$, 1.7 and 1.8 (Fig. 6). The fine structure of both the V-$L_{2,3}$ edge (520 eV and 513 eV) and the O-K edge (532 eV) is known to be valence- and coordination-sensitive in vanadates. Three reference vanadium oxides, V_2O_3, V_2O_4 and V_2O_5, were therefore also measured to allow a direct comparison between our materials and the references. Judging by the onset and shape of the V-$L_{2,3}$ edge, the vanadium in all three samples ($x = 1.6$, 1.7 and 1.8) appears to have a very similar electronic state, being mainly a mixed V^{3+}/V^{4+} one, whereby the presence of small amounts of V^{5+} is recognizable in particular at x = 1.6.

Physical properties

The impact of this simultaneaous filling of channels on magnetic and transport properties has been investigated in the case of $Bi_xV_8O_{16}$, with the nominal x values of 1.6 and 1.8. Magnetic susceptibility measured in a field of 100Oe is presented in Figure 7 for the two x values. These measurements are consistent with the ones previously reported in [7], with very low values of χ in the whole field range ($\approx 10^{-2}$ emu/mol), a high T maximum of χ close to 200 – 250 K typical of low dimensional magnets, and a low-T upturn at 60 K. For x = 1.6, χ is characteristic of a Pauli paramagnet. In the case of x = 1.8, the low-T upturn at 60 K is very sharp. NMR experiments have shown that it can be attributed to the presence of V^{3+} - V^{3+} pairs, coexisting with V^{4+} paramagnetic spins [8]. The temperature of 60 K corresponds as well to the metal-to-insulator transition as observed in the inset of Figure 7 for x = 1.8, with a strong increase of ρ observed below 60 K, when entering in the spin singlet phase [8-9]. On the

other hand, the x = 1.6 sample exhibits only a moderate increase of ρ by two orders of magnitude down to 2 K, in contrast with the 8 orders of magnitude observed for x = 1.8. The values of resistivity and the large differences observed between x = 1.6 and x = 1.8 are in good agreement with the ones previously published[7]. Above 200 K, both materials exhibit very small values of ρ of few mΩ·cm, almost constant up to 950 K.

The thermopower of $Bi_xV_8O_{16}$ is presented in Figure 8. The values are negative in the whole temperature range (5 – 950 K) for the two x concentrations. The magnitude of S continuously increases up to 1000 K, to ~ 35- 40µV·K^{-1}. In the two curves, S presents a minimum in magnitude at approx. 150 K, followed by a rapid increase of $|S|$ below 150 K. In the most insulating compound (x = 1.8), S can be measured only down to 40 K, and the transition at 60 K is observed, with a more rapid increase of $|S|$ below 60 K, as shown by the dashed line in Figure 8. On the other hand, in the case of the more metallic $Bi_{1.6}V_8O_{16}$, S can be measured down to 5 K. A clear transition is observed at 60 K, and S tends to zero, with a linear behavior characteristic of a metal below 15K.

Above 200 K, these two curves are similar to the one of $Pb_{1.6}V_8O_{16}$ previously reported [10], with S close to -40 µV·K^{-1} at 900 K, and a sharp increase of $|S|$ below 140 K. This sharp increase had been attributed to the occurrence of charge and orbital ordering, also observed on the resistivity curve. The electrical and magnetic transition observed at 60 K for x = 1.8 has the same impact on S, with an increase of the slope d$|S|$/dT below 60 K. The minimum of χ(T) at 60 K corresponds to the low-T transition in S(T) (shown by the dashed line in figure 8). For x = 1.8, the transition towards a more resistive behavior observed at 60 K has thus a direct impact on S, as expected, but the thermopower measurements suggest a possible second transition at 150 K, which would be very similar to the one at 140 K in $Pb_{1.6}V_8O_{16}$. The possible origin of this transition is not clear and will deserve further investigation. It must also be stressed that, even if ρ increases at low T for x = 1.6, the increase is not as steep as for x = 1.8 and the S(T) curve is characteristic of a metallic transport down to low T, suggesting a different low T ground state for x = 1.6. The magnetic transition at 60K is also smoother than for x = 1.8,

These Seebeck experiments raise several questions. First of all, in a simple picture of V^{4+} carriers doped in a V^{3+} matrix, thermopower should be positive. This is not the case, as previously shown in $Pb_{1.6}V_8O_{16}$. According to the Heikes equation $S = \dfrac{-k_B}{e} \ln(\dfrac{1-x}{x})$ as more carriers are introduced[34], the magnitude of S should decrease, but the magnitude of S

actually does not change significantly. The thermopower needs thus to be described in a more complex manner. The high-T Seebeck tends to -35 $\mu V \cdot K^{-1}$ and, as previously discussed[10], this is very close to the spin entropy term associated to a mixed valence of V^{3+} ($3d^2$) / V^{4+} ($3d^1$). Considering a generalized Keikes formula [35], a spin and orbital entropy term has to be added to the calculation of S with $S = \dfrac{-k_B}{e} \ln(\dfrac{1-x}{x}) - \dfrac{k_B}{e} \ln(\dfrac{g_3}{g_4})$, where $g_3 = \Gamma_{orb}(V^{3+})$ $\Gamma_{spin}(V^{3+})$ and $g_4 = \Gamma_{orb}(V^{4+}) \Gamma_{spin}(V^{4+})$ reflect the orbital and spin degeneracy terms for V^{3+} and V^{4+}, respectively. In these hollandites, S seems to be dominated by the spin entropy term, which is equal to $\dfrac{-k_B}{e} \ln(\dfrac{(2S_{V3+}+1)}{(2S_{V4+}+1)}) = \dfrac{-k_B}{e} \ln(\dfrac{3}{2}) = -35 \mu V \cdot K^{-1}$, S_{V3+} and S_{V4+} being the spins of V^{3+} and V^{4+}. This predominance of spin entropy has already been observed in ruthenates such as $SrRuO_3$[36] or Sr_2RuO_4, and has been related to the freezing of orbital fluctuations up to 950 K [37], revealing the dominant role of spin entropy on the thermopower in this temperature range. It would be interesting to determine if such a freezing of orbital fluctuations could also be at play in these vanadium hollandites.

The presence of two transitions in S(T) at ≈60 K and 150 K is puzzling. The one at 60 K can be related to the minimum of magnetic susceptibility, but the one at 150 K does not correspond to any other transition reported so far, and looks very similar to the one of $Pb_{1.6}V_8O_{16}$, and almost at the same temperature. Due to the low-dimensional nature of the hollandites, the magnetic fluctuations could play a crucial role on transport in a broad range of temperature as discussed above, and the thermopower is often a very sensitive probe of these fluctuations. Further work is needed to better understand the low-temperature transitions.

To conclude, resistivity measurements show metal-to-insulator transitions at low T (T = 60 K) observed both for x = 1.6 and x = 1.8, the transitions being much sharper for x = 1.8, while the thermopower measurements suggest a more metallic ground state for x = 1.6 at low T. The magnetic transition at 60K is also much sharper for x = 1.8. On the other hand, the thermopower and resistivity are not very sensitive to x at high T, and the thermopower seems to be dominated by the spin entropy associated to V^{3+} / V^{4+} in this T range.

New features of the-$Bi_xV_8O_{16}$ hollandite

The present study points towards different new features for the $Bi_xV_8O_{16}$ hollandite. For T > 200 K, the electrical resistivity is x- and T-independent with values remaining all close to few mΩ·cm. This semi-metallic behavior is accompanied with a negative Seebeck coefficient

which absolute |S| value increases with T. At the highest measured T (950 K) S values are very close for x = 1.6 and x = 1.8 with S ≈ -35μV·K^{-1}. This suggests that S is dominated by the spin entropy term related to V^{3+} and V^{4+} when orbitals fluctuations are frozen and that the V formal valency calculated from the nominal Bi$_{1.6}$V$_8^{3.4+}$O$_{16}$ and Bi$_{1.8}$V$_8^{3.32+}$O$_{16}$ compositions is very close. These behaviors at high T contrast with the very different magnitude of the metal-to-insulator transition at $T ≈ 60$ K when one compares the x = 1.6 and x =1.8 samples. The χ- and ρ-coupled changes at T_{MI} are much more pronounced in Bi$_{1.8}$V$_8$O$_{16}$ than in Bi$_{1.6}$V$_8$O$_{16}$, and thermopower measurements reveal a metallic ground state at low T for x = 1.6. However, from EELS it is not possible to detect a significant change in the effective valence v_V as x increases from 1.6 to 1.8. The transition at 60 K is believed to be related to the fact that for $x = 1.8$, v_V should be very close to 3.33, which is consistent with the existence of a 1:2 ratio for charge and orbital ordering invoked to explain the MIT as proposed in Ref. 7-9 and evidenced by NMR showing a coexistence of spin-singlet V^{3+}-V^{3+} with V^{4+} having a localized spin moment. Even though a V$^{3.33+}$ oxidation favors a concomitant charge and orbital ordering in the (VO$_6$)$_2$ stripes, lifting the triangular degeneracy, due to the electronic repulsion between the cations in the tunnel and extra charges of the neighboring stripes, it is expected that the *A* cations and vacancies tend to order. Thus, the possibility to get ordered or disordered chains of Bi^{3+} and vacancies in the large square tunnels is an important issue.

In that respect, the TEM study gives a different scenario about the filling up in the channels of the hollandite structure. Combining HAADF-STEM and image simulations data based on local structural models and supported by DFT calculations, it is demonstrated that the wider channels of the structure are mostly partially occupied by Bi^{3+} cations and this partial occupation is locally accompanied by extra vanadium cations shifted from the center of these channels. This compensation mechanism by replacement toward a virtual limit composition 'M$_2$M$_8$O$_{16}$' could also be at play in hollandites of other M metals. With such a mechanism, the formal metal oxidation state of the hollandite Bi$_{2-y}$V$_y$V$_8$O$_{16}$ could be kept constant: considering the actual compositions Bi$_{1.6}$V$_{8.4}$O$_{16}$ and Bi$_{1.8}$V$_{8.2}$O$_{16}$ for the x = 1.6 and x =1.8 samples of our study, one obtains v_V = 3.23 and v_V = 3.24, respectively. As the V species in the tunnels are in tetrahedral coordination, one could also consider pentavalent vanadium in tetrahedral coordination which yields different v_V for the vanadium cation in the (VO$_6$)$_2$ stripes, (Bi$_{1.6}$V$_{0.4}^{5+}$)V$_8^{3.15+}$O$_{16}$ and (Bi$_{1.8}$V$_{0.2}^{5+}$)V$_8^{3.20+}$O$_{16}$. Note that the corresponding cation ratio differ from the nominal ones. Nevertheless, this shift is very limited, with a Bi/V ratio equal to 0.220 and 0.225 for 'Bi$_{1.8}$V$_8$' and 'Bi$_{1.8}$V$_{8.2}$' respectively. Also, the presence of

vacancies in the tunnels cannot be completely ruled out. Though our observations do not allow the exact quantification of Bi, V and vacancies in the tunnels, they point towards differences in the electronic repulsion between these species and the extra charges on the V-O network of the neighboring stripes. Especially, as the number of V species in the tunnel increases as y increases according to an idealized $(Bi_{2-y}V_y)V_8O_{16}$ chemical formula, the charge and orbital ordering in the V_8O_{16} framework should be hindered. This disorder effect would explain the more pronounced transitions observed for the x = 1.8 sample than for the x = 1.6 one, rather than a pure electronic scenario related to the v_V shift from 3.3 as one goes from $Bi_{1.8}V_8^{3.325+}O_{16}$ to $Bi_{1.6}V_8^{3.475+}O_{16}$.

Conclusion

The TEM study of the hollandite $Bi_xV_8O_{16}$ revealed the presence of additional V species located together with Bi in the channels of the crystal structure. The vanadium fillers occupying off-centered atomic positions in the channels have tetrahedral coordination (V^{5+}) differently from the octahedral one (V^{3+}, V^{4+}) in the V_8O_{16} framework. The average value of the vanadium oxidation state calculated from the new model of this hollandite differs from that obtained by considering the nominal composition $Bi_xV_8O_{16}$. As a consequence, rather x-independent value of the Seebeck coefficient S could be attributed to the new vanadium oxidation state which exhibits an x-independent value. In contrast, the disorder introduced from channel to channel by the coexisting V and Bi could impact the setting of the charge and orbital ordering, explaining why the transition is smeared out when the Bi nominal content x decreases. The question now is to understand if this concomitant filling of the channels by Bi^{3+} and vanadium is related to the Bi^{3+} lone pair and/or the versatility of vanadium to adopt different coordination and oxidation states in oxides. Considering the potential applications of these hollandites for nuclear waste storage, electrodes, or as photocatalysis, these results highlight the importance of a local investigation of the channels to better understand the relationship between the octahedra network and the channel fillers, and thus better understand the doping mechanism and the disorder influence.

Acknowledgments

References

1. Isobe, M.; Koishi, S.; Yamazaki, S.; Yamaura, J.; Gotou, H.; Yagi, T.; Ueda, Y., Substitution Effect on Metal–Insulator Transition of $K_2V_8O_{16}$, *J. Phys. Soc. Jpn.* **2009**, *78*, 114713.

2. Isobe, M.; Koishi, S.; Kouno, N.; Yamaura, J.; Yamauchi, T.; Ueda, H.; Gotou, H.; Yagi, T.; Ueda, Y., Observation of Metal–Insulator Transition in Hollandite Vanadate, $K_2V_8O_{16}$, *J. Phys. Soc. Jpn* **2006**, *75*, 073801.

3. Toriyama T., Nakao A., Yamaki Y., Nakao H., Murakami Y., Hasegawa K., Isobe M., Ueda Y., Ushakov A. V., Khomskii D. I. , Streltsov S. V., Konishi T., Ohta Y., Peierls Mechanism of the Metal-Insulator Transition in Ferromagnetic Hollandite $K_2Cr_8O_{16}$, *Phys. Rev. Lett.* **2011**, *107*, 266402.

4. Kuwabara, T.; Isobe, M.; Gotou, H.; Yagi, T.; Nishio-Hamame, D.; Ueda, Y., Synthesis, Structure, and Electromagnetic Properties of Manganese Hollandite, $K_xMn_8O_{16}$, *J. Phys. Soc. Jpn.* **2012**, *81*, 104701.

5. Ozawa, T.; Suzuki, I.; Sato, H., Structural, Magnetic and Electronic Transport Properties of Novel Hollandite-Type Molybdenum Oxide, $Rb_{1.5}Mo_8O_{16}$, *J. Phys. Soc. Jpn* **2006**, *75*, 014802.

6. Sato, H.; Enoki, T.; Yamaura, J.; Yamamoto, N., Charge localization and successive magnetic phase transitions of mixed-valence manganese oxides $K_{1.5}(H_3O)_xMn_8O_{16}$ $0<x<0.5$, *Phys. Rev. B* **1999**, *59*, 12836- 12841.

7. Kato, H.; Waki, T.; Kato, M.; Yoshimura, K.; Kosuge, K., Temperature-Induced Metal-Insulator Transition in $Bi_xV_8O_{16}$, *J. Phys. Soc. Jpn.* **2001**, *70*, 325- 328.

8. Waki, T.; Kato, H.; Kato, M.; Yoshimura, K., Metal–Insulator Transition in $Bi_xV_8O_{16}$: [51]V NMR Study, *J. Phys. Soc. Jpn* **2004**, *73*, 275 – 279.

9. Waki, T.; Kato, M.;Yoshimura, K., Observation of spin-singlet state in $Bi_xV_8O_{16}$, *Physica B* **2005**, *359 – 361*, 1309- 1311.

10. Maignan, A.; Lebedev, O.I.; Van Tendeloo, G.; Martin, C.; Hébert, S., Metal to insulator transition in the *n*-type hollandite vanadate $Pb_{1.6}V_8O_{16}$, *Phys. Rev. B* **2010**, *82*, 035122.

11. Ishiwata S., Bos J. W. G., Huang Q., Cava, R. J., Structure and magnetic properties of hollandite $Ba_{1.2}Mn_8O_{16}$, *J. Phys.: Condens. Matter* **2006**, *18*, 3745–3752.

12. Crespo, Y.; Andreanov, A.; Seriani, N., Competing antiferromagnetic and spin-glass phases in a hollandite structure, *Phys. Rev. B* **2013**, *88*, 014202.

13. Larson A. M. , Moetakef P., Gaskell K., Brown C. M., King G. and Rodriguez E. E., Inducing Ferrimagnetism in Insulating Hollandite $Ba_{1.2}Mn_8O_{16}$, *Chem. Mater*. **2015**, *27*, 515 -525.

14. Sooran Kim S., Kim B. H., Kim K., Min B. I., Metal-insulator transition in a spin-orbital-lattice coupled Mott system: $K_2V_8O_{16}$, *Phys. Rev. B* **2016**, *93*, 045106.

15. Huang, J.; Poiraz, A.S.; Takeuchi, K.J.; Takeushi, E.S.; Marschilok, A.C. $M_xMn_8O_{16}$ (M = Ag or K) as promising cathode materials for secondary Mg based batteries: the role of the cation M, *Chem. Comm* **2016,** *52*, 4088- 4091.

16. Mori T., Yamauchi S., Yamamura H., Watanabe M. , New hollandite catalysts for the selective reduction of nitrogen monoxide with propene, *Applied Catalysis A* 1995, 129, L1 – L7.

17. Krishna, SR, Shrujana, P, Palla, S, Sreenu, K, Velchuri, R, Vithal, M. , Preparation, characterization and photocatalytic studies of $K_2Al_2Ti_6O_{16}$, $K_{2-x}Ag_xAl_2Ti_6O_{16}$ and $K_2Al_2Ti_6O_{16-x}N_y$, *Materials Research Express* **2015,** *2,* 035008.

18. Bursill, L.A.; Smith, J., Electron irradiation effects in (Cs, Ba) – hollandites, *J.Solid State Chem*. **1987**, *69*, 343- 354.

19. Tumurugoti P,, Clark B. M., Edwards D. J., Amoroso J., Sundaram S. K., Cesium incorporation in hollandite-rich multiphasic ceramic waste forms, *J. Solid Stat. Chem.* **2017**, 246, 107 -112.

20. Wu, L.; Xu, F.; Zhu, Y.; Brady, A.B.; Huang, J.; Durham, J.L.; Dooryhee, E.; Marschilok, A.C.; Takeuchi, E.S.; Takeuchi, K.J., Structural Defects of Silver Hollandite, $Ag_xMn_8O_y$, Nanorods: Dramatic Impact on Electrochemistry, *ACS Nano* **2015**, *9*, 8430- 8439.

21. Laurita G ., Grajczyk R., Stolt M., Coutinho I., Sleight A. W., Subramanian M. A., Influence of Structural Disorder on Hollandites $A_xRu_4O_8$ (A^+ = K, Rb, $Rb_{1-x}Na_x$), *Inorg. Chem.* **2016**, *55*, 3462−3467.

22. Carter, M.L., Withers, R.L., An electron and X-ray diffraction study of the compositely modulated barium nickel hollandite $Ba_x(Ni_xTi_{8-x})O_{16}$, 1.16 < x < 1.32, solid solution, *Z.Kristallogr.* **2004**, *219*, 763- 767.

23. Carter, M.L., Withers, R.L., A universally applicable composite modulated structure approach to ordered $Ba_xM_yTi_{8-y}O_{16}$ hollandite-type solid solutions, *J. of Solid State Chem* **2005**, *178*, 1903 - 1914.

24. Nistor, L.C., Van Tendeloo, G., Amelinckx, S., Defects and phase transitions in natural monoclinic hollandite: $Ba_xMn_8O_{16}$, *J. of Solid State Chem* **1994**, *109*, 152- 165.

25. Mentré, O., Abraham, F. New Mixed Valence Compounds in the Pb–V–O System: Synthesis and Crystal Structure of Hollandite-Related $Pb_{1.32}V_{8.35}O_{16.7}$ and *R*-Type Hexagonal Ferrite PbV_6O_{11}, *J. of Solid State Chem* **1996,** *125*, 91 - 101.

26. Abraham, F.; Mentré, O. $Bi_{1.7}V_8O_{16}$ – The first Bi- hollandite type compound, *J. of Solid State Chem* **1994**, *109*, 127- 133.

27. Momma, K.; Izumi, F., VESTA 3 for three-dimensional visualization of crystal, volumetric and morphology data, *J. Appl. Crystallogr* **2011**, *44*, 1272- 1276.

28. Koch, C.T. **2002** Determination of core structure periodicity and point defect along dislocations *PhD thesis* Arizona State University.

29. Kresse, G.; Hafner, J. Ab- initio molecular dynamics for liquid metals, *Phys. Rev. B* **1993**, *47***,** 558- 561.

30. Kresse, G.; Furthmüller, J., Efficient iterative schemes for ab initio total-energy calculations using a plane-wave basis set, *Phys. Rev. B* **1996**, *54***,** 11169- 11186.

31. Perdew, J.P.; Burke, K.; Ernzerhof, M., Generalized gradient approximation made simple, *Phys. Rev. Lett* **1996,** *77***,** 3865- 3868.

32. Blöchl, P.E., Projector augmented- wave method, *Phys. Rev B.* **1994,** *50***,** 17953- 17979.

33. Hytch, M.J.; Snoeck, E.; Kilaas, R. Quantitative measurement of displacement and strain fields from HREM micrographs, *Ultramicroscopy* **1998**, *74*, 131- 146.

34. Chaikin, P.M.; Beni, G., Thermopower in the correlated hopping regime, *Phys. Rev. B* **1976**, *13*, 647- 651.

35. Koshibae, W.; Tsutsui, K.; Maekawa, S., Thermopower in cobalt oxides, *Phys. Rev. B* **2000**, *62*, 6869- 6872.

36. Klein, Y.; Hébert, S.; Maignan, A.; Kolesnik, S.; Maxwell, T.; Dabrowski, B., Insensitivity of the band structure of substituted $SrRuO_3$ as probed by Seebeck coefficient measurements, *Phys. Rev. B* **2006**, *73*, 052412.

37. Mravjle, J.; Georges, A., Thermopower and Entropy: Lessons from Sr_2RuO_4, *Phys. Rev. Lett.* **2016***, 117,* 036401.

Figure Legends

Fig 1: a) Powder XRD pattern of $Bi_{1.6}V_8O_{16}$ (space group $I4/m$) with the indexation of the first Bragg peaks. Insert: b) VO_6 octahedra (blue) highlighting the narrow and wide tunnels containing Bi cations (red) in a perspective view along the [001] direction and c) the triangular ladder-like vanadium sublattice (yellow) with the shortest V-V distances (in Å) in a view along [100]

Fig. 2: ED patterns and HRTEM image of $Bi_{1.8}V_8O_{16}$: (a) ED patterns along the main zone axes [001] , [100] and [111]. Notice appearance of diffuse linear reflections in the [100] and [111] ED patterns marked by white arrows; (b) [001] HRTEM image and an enlargement with overlapped structural model as insert.

Fig. 3: HRTEM on $Bi_{1.8}V_8O_{16}$:

(a) [001] High resolution HAADF-STEM image with an enlargement and structural overlay model in insert (Bi – brown, V-yellow, O-blue).

(b) [100] High resolution HAADF-STEM image and corresponding FT pattern, notice diffuse scattering around 0hl spots similar to that of ED in Fig 2a.

(c) Enlargement of selected area in (b) and corresponding intensity plot profile along Bi row (marked with white arrows) indicating presence of differently occupied Bi columns. The columns with the Bi deficiency depicted with white arrowhead in the figure and black arrow in the intensity plot profile.

(d) Enlargement image of [100] HAADF-STEM overlaid with structural model (Bi – brown, V-yellow, O-blue). Notice splitting Bi atoms due to A-cation split position with partial occupancy reported for $Bi_{1.625}V_8O_{16}$ [25 -26]. Red arrows head pointed out the absence one of the two Bi atoms in some columns.

Fig. 4: Experimental (cf. Figure 4a) and simulated HAADF-STEM images of $Bi_{1.8}V_8O_{16}$ based on structural models of different atomic arrangements in the wide channels: (a) model 1 (no bismuth defects on the 00z and ½½z axes, composition $Bi_2V_8O_{16}$) in projection along [001] and [100] directions; (b) model
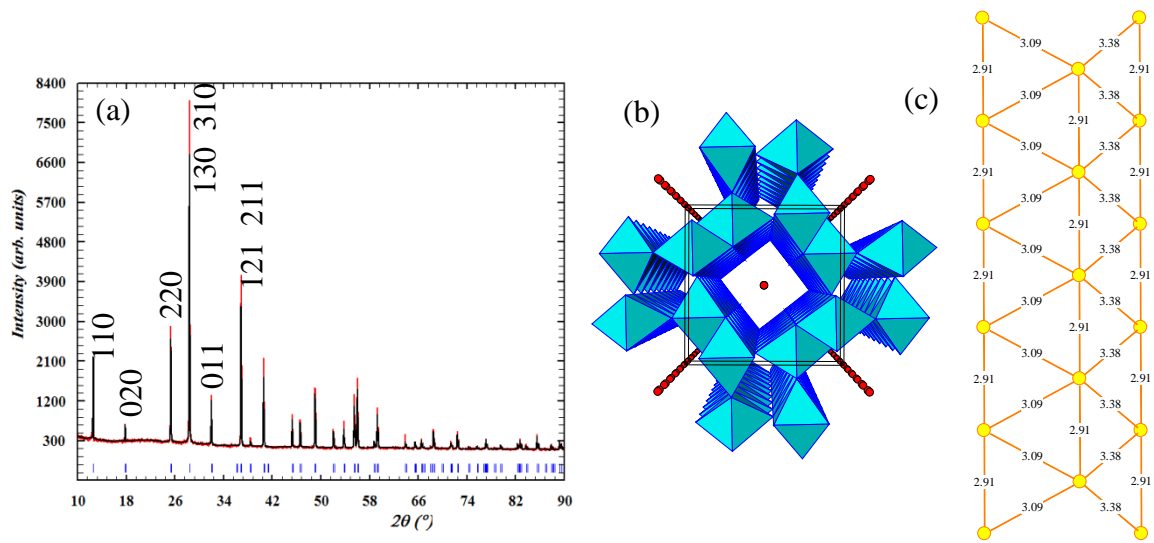
2 (complete bismuth absence on the channel axis ½½z, replaced by the vanadium atoms located at the wall of the tunnel, composition $Bi_1V_1V_8O_{16}$) in projection along [001] and [100] directions; (c) model 3 (mixed occupation of the channel axis ½½z with V/Bi ratio 3/1, composition $Bi_{1.25}V_{0.75}V_8O_{16}$) in projection along [001] and [100] directions; (d) model 4 (mixed occupation of the channel axis ½½z with V/Ba ratio 1/1, composition $Bi_{1.5}V_{0.5}V_8O_{16}$) in projection along [001] and [100] directions.

Fig. 5:   The line defect structure of $Bi_{1.75}V_{0.25}V_8O_{16}$ in the ball-and-stick representation as revealed by density functional theory calculations. A column of Bi atoms (brown balls) was replaced by V atoms (yellow). Blue dashed line shows the periodic supercell used in the calculations (top orthographic view). The panel on the right-hand side shows the details of the atomic structure in the defect area (perspective view).

Fig. 6:   Energy loss near edge spectra of V-$L_{2,3}$ edge and O-K edge of three V oxide references together with the investigated samples $Bi_xV_6O_{18}$ (x=1.8, x=1.7, x=1.6). The onset of the V-$L_{2,3}$ edge and the shape of both the V-$L_{2,3}$ and O-K fine structures indicate the electronic state of V in $Bi_xV_6O_{18}$ being mainly a mixture of V^{3+} and V^{4+} with small contributions of V^{5+}.

Fig. 7:   Magnetic susceptibility χ(T) measured in a field of 100 Oe for x = 1.6 (squares) and x = 1.8 (triangles). Inset: Electrical resistivity of $Bi_xV_8O_{16}$ measured up to 950 K for x = 1.6 (squares) and x = 1.8 (triangles).

Fig. 8:   Seebeck coefficient of $Bi_xV_8O_{16}$ measured up to 950 K for x = 1.6 (squares) and x = 1.8 (triangles). These values are compared to the ones of $Pb_{1.6}V_8O_{16}$ previously reported [9] (stars). The dashed line corresponds to T = 60 K, i. e. the metal-to-insulator transition temperature.

1
2
3
4
5
6
7
8
9
10
11
12
13
14
15
16
17
18
19
20
21
22
23
24
25
26
27
28
29
30
31
32
33
34
35
36
37
38
39
40
41
42
43
44
45
46
47
48
49
50
51
52
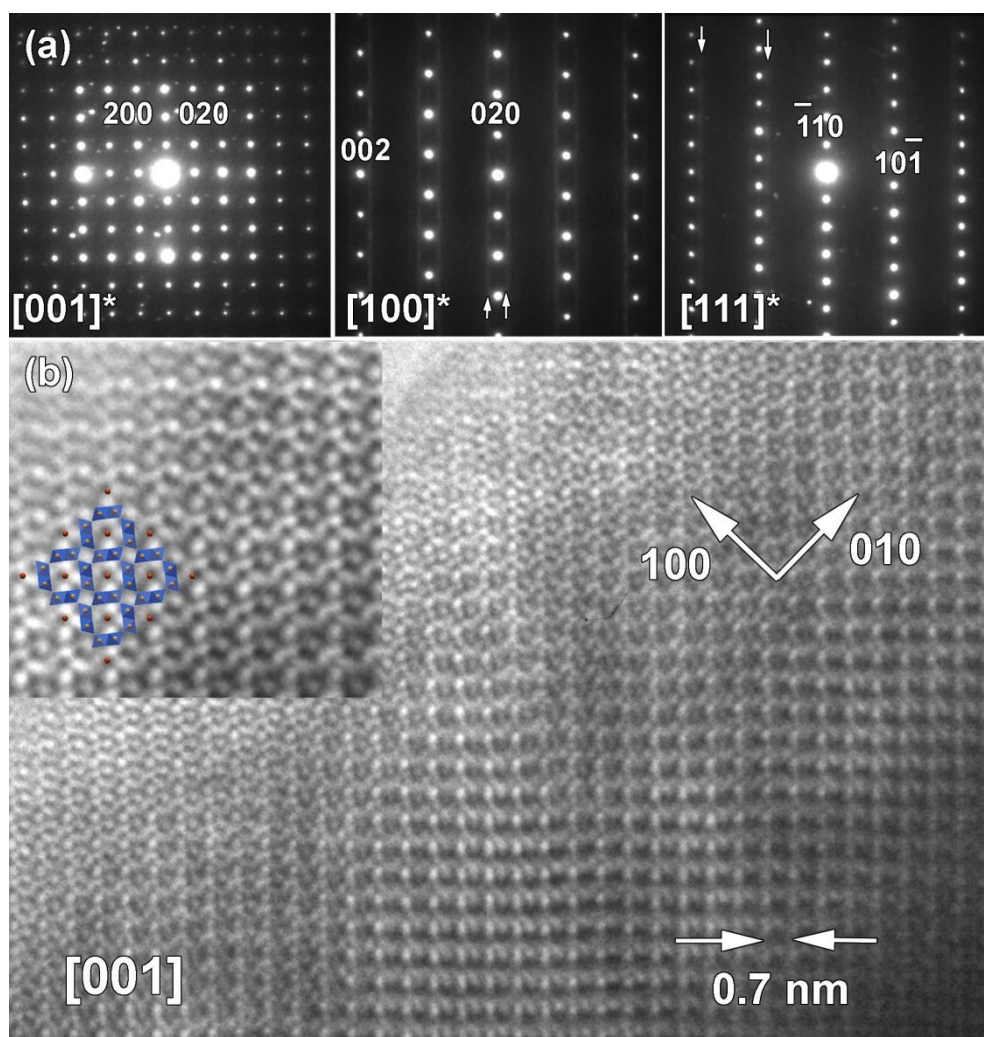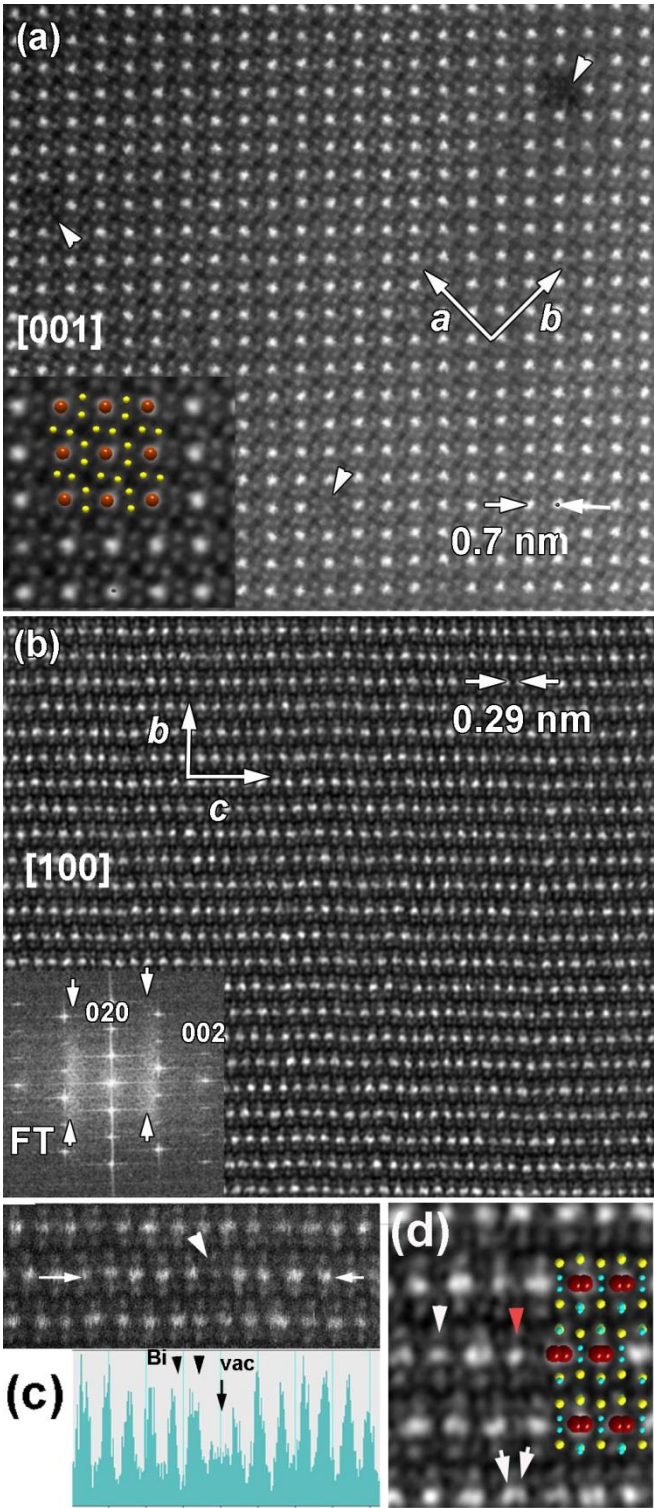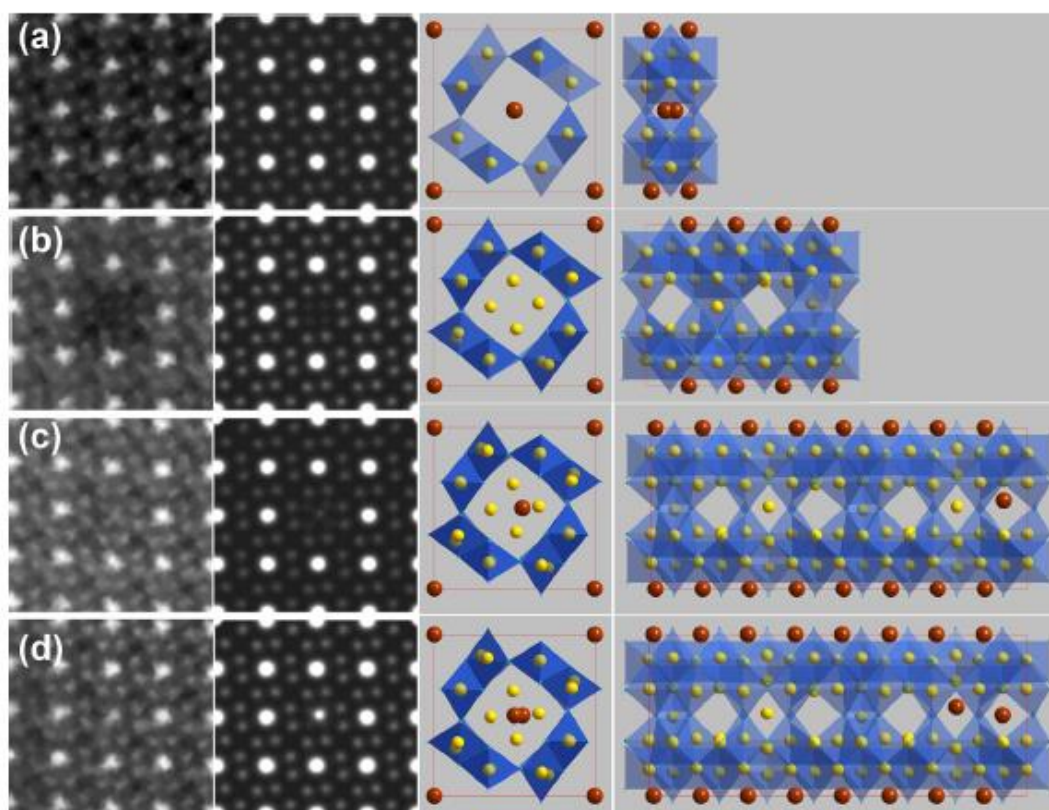53
54
55
56
57
58
59
60

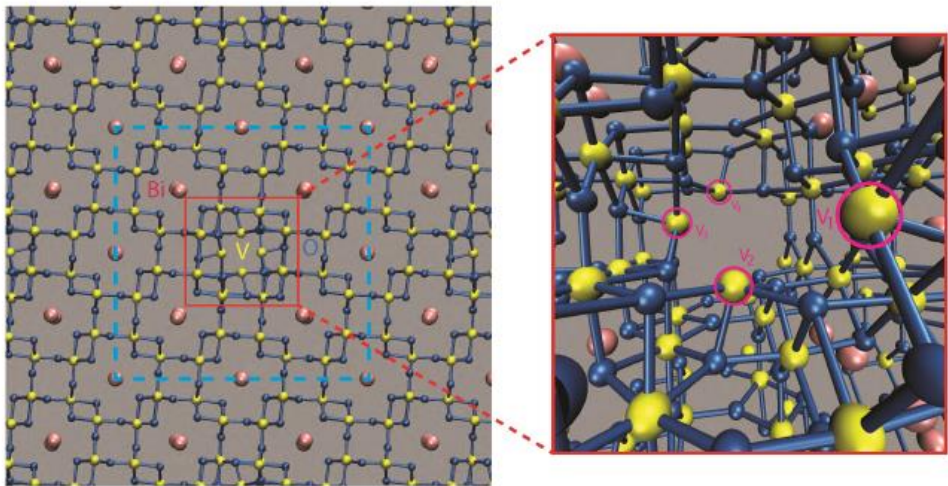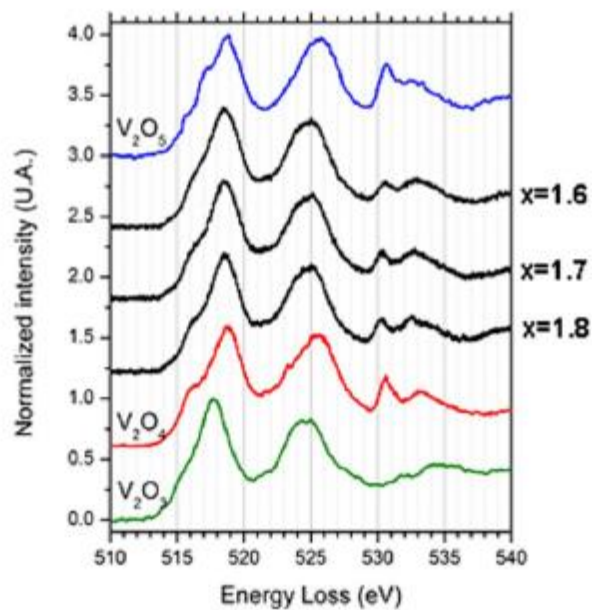(a) Intensity (arb. units) vs 2θ (°)

(b)

(c)

Figure 2

Figure 3

Figure 4

Figure 5

Figure 6

Figure 7

Figure 8